Research Article

Mageswari Manimaran, Mohd Nurazzi Norizan*, Mohamad Haafiz Mohamad Kassim, Mohd Ridhwan Adam, Norli Abdullah, and Mohd Nor Faiz Norrrahim*

Surfaces and interfaces analysis on different carboxymethylation reaction time of anionic cellulose nanoparticles derived from oil palm biomass

https://doi.org/10.1515/ntrev-2025-0152
received December 8, 2024; accepted March 2, 2025

Abstract: Recent advancements in nanotechnology have expanded the applications of cellulose nanoparticles (CNPs) isolated from various types of biomass waste like oil palm empty fruit bunches. These applications are particularly enhanced by incorporating nanoparticles or polymers. However, a significant challenge in synthesizing CNP-based nanocomposites lies in the selection of appropriate synthesis methods, as ineffective techniques can result in poor compatibility between nanoparticles. To overcome this issue, surface modification through carboxymethylation has emerged as an effective strategy. This process introduces anionic groups ($-CH_2COONa^+$) onto the CNP surface, producing anionic nanocellulose particles (ACNPs) that act as capping agents to enhance nanoparticle incorporation. Despite these advancements, the optimum reaction time for isolating ACNPs from CNPs, particularly nanocrystalline cellulose, remains underexplored. This study investigates the effect of varying carboxymethylation reaction times (30 min, 2, 4, 6, and 8 h) on the synthesis of ACNPs. Characterization techniques, including Fourier transform infrared (FTIR) spectroscopy, X-ray diffraction, transmission electron microscopy, zeta potential analysis, thermogravimetric analysis, Raman spectroscopy, and X-ray photoelectron spectroscopy (XPS), were employed. The results indicate that a reaction time of 4 h is optimal for carboxymethylation. ACNPs synthesized at this duration exhibit good dispersion, improved thermal stability, and a high zeta potential value (−41 mV) compared to CNPs (−25 mV). FTIR analysis reveals new peaks at 1,564, 1,432, and 1,321 cm^{-1}, corresponding to the carboxyl, methyl ($-CH_2$), and hydroxyl groups of the carboxymethyl group ($-CH_2$–COONa), respectively. Additionally, XPS results show a high concentration of Na^+ ions in ACNPs synthesized at 4 h. Beyond this reaction time, Na^+ concentration decreases.

Keyword: nanocellulose, oil palm empty fruit bunch, carboxymethylation reaction

*** Corresponding author: Mohd Nurazzi Norizan**, Bioresource Technology Division, School of Industrial Technology, Universiti Sains Malaysia, Penang, 11800, Malaysia; Green Biopolymer, Coatings & Packaging Cluster, School of Industrial Technology, Universiti Sains Malaysia, Penang, 11800, Malaysia, e-mail: mohd.nurazzi@usm.my
*** Corresponding author: Mohd Nor Faiz Norrrahim**, Research Center for Chemical Defence, Defence Research Institute, Universiti Pertahanan Nasional Malaysia, Kem Perdana Sungai Besi, Kuala Lumpur, 57000, Malaysia, e-mail: faiz@upnm.edu.my
Mageswari Manimaran, Mohamad Haafiz Mohamad Kassim: Bioresource Technology Division, School of Industrial Technology, Universiti Sains Malaysia, Penang, 11800, Malaysia; Green Biopolymer, Coatings & Packaging Cluster, School of Industrial Technology, Universiti Sains Malaysia, Penang, 11800, Malaysia
Mohd Ridhwan Adam: School of Chemical Sciences, Universiti Sains Malaysia, Penang, 11800, Malaysia
Norli Abdullah: Centre for Defence Foundation Studies, Universiti Pertahanan Nasional Malaysia, Kem Perdana Sungai Besi, 57000, Kuala Lumpur, Malaysia

1 Introduction

Oil palm is the most cultivated plant in Malaysia with approximately 5.65 million hectares of planted area and also with annual production of crude palm oil production around 18.55 million metric tons according to the 2023 statistic [1]. At the same time, there has been a significant increase in biomass waste from plantations and milling activities, as illustrated in Figure 1. Oil palm biomass produced from plantations includes oil palm trunks and oil palm fronds, while milling operations generate additional biomass such as oil palm empty fruit bunches (OPEFB), mesocarp fibre, and palm kernel shells. Annually, approximately 127 million tons of oil palm biomass are generated, presenting substantial environmental and economic

Figure 1: The statistics of oil palm biomass generated in Malaysia annually.

challenges that require immediate attention [2]. If left unmanaged, this enormous volume of biomass could contribute to deforestation, air pollution, and greenhouse gas emissions, further exacerbating climate change.

Therefore, it is crucial to implement efficient and eco-friendly solutions to mitigate potential harm and unlock the full potential of these resources for renewable energy, waste reduction, and other beneficial uses. Hence, the development of advanced materials with superior properties has led to the significant interest of researchers in utilizing oil palm biomass in various applications in order to produce a valuable product from oil palm biomass. One of the valuable products from the oil palm biomass is the nano-scaled sized materials known as nanocellulose, which has superior properties such as high reinforcing strength and stiffness, which is often times comparable to Kevlar and steel, large surface area, remarkable optical properties, tailored crystallinity, and easy surface functionalization due to abundance of hydroxyl groups (−OH) [3]. Not only that, due to its high surface area and biocompatibility, nanocellulose from oil palm biomass has become particularly promising materials as a bio-reinforcing filler or in the production of biopolymer composites [4,5]. The incorporation of the cellulose nanoparticles (CNPs) with different types of nanoparticles can improve mechanical, thermal, and electrical properties, which exhibit unique characteristics that differ from the bulk counterparts [4].

However, very limited studies are conducted by researchers on the incorporation of different types of nanoparticles such as metal oxide or carbon-based with oil palm-based CNPs to produce nanocomposite rather than film and polymer-nanocomposite. This is mainly due to the −OH group on the CNP surface, which resulting issues of agglomeration, poor dispersion, and compatibility, which should be addressed in order to produce a high-quality nanocomposite [6]. Metal oxide nanoparticles may be separately synthesized and added to nanocellulose (*ex situ* processes), or they can be synthesized using nanocellulose as a template (*in situ* processes) [7]. In the latter case, the precursor is trapped inside the CNP network and then reduced to metal oxide.

As a result, concern about the synthesis and functionalization method of nanocomposite is crucial as it can help overcoming the issue mentioned above. There are four ways to synthesize the nanocomposite: (1) simple blending, (2) by the external reducing agent, (3) surface modification, and lastly, (4) without an external reducing agent, as shown in Figure 2 [8]. The most widely used method based on recent studies is surface modification for film production and bio-composite synthesis. The

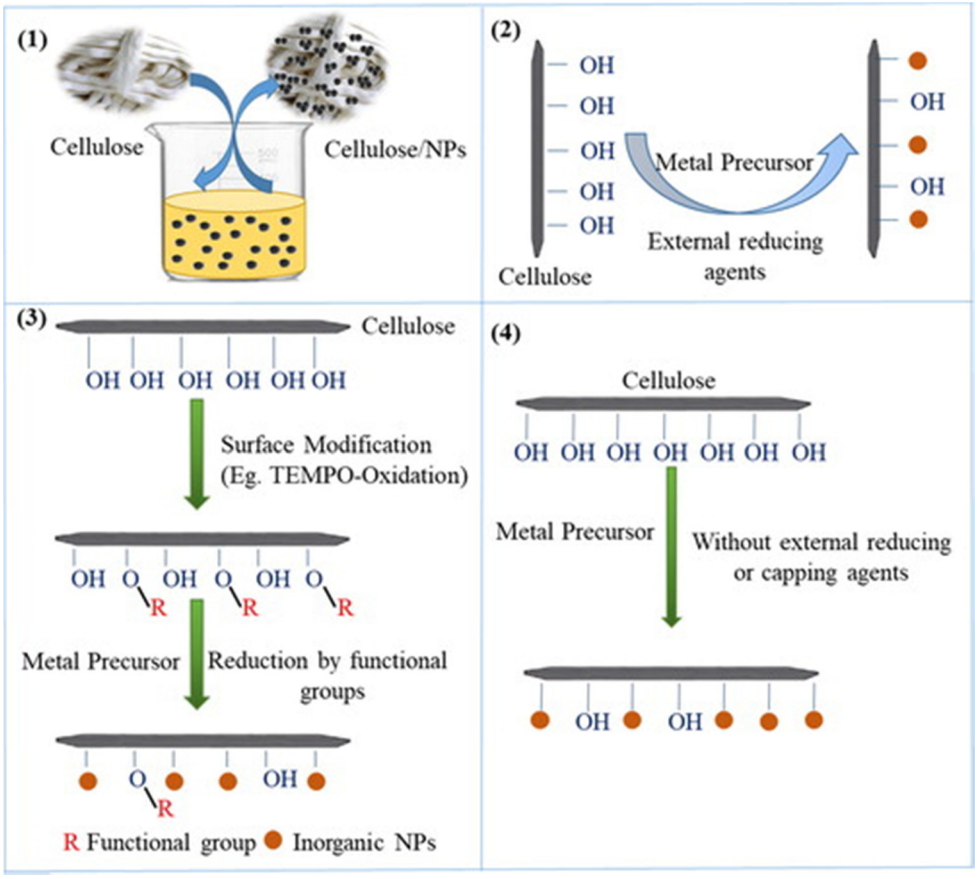

Figure 2: Four methods to synthesize nanocomposite: (1) simple blending, (2) by using an external reducing agent, (3) surface modification, and lastly (4) using without external reducing agent. Reproduced from ref. [8].

surface chemical modification methods of CNPs can be divided into two, which are (a) chemical modification (esterification, silylation, cationization, treatment with isocyanates, and so on) or (b) grafting macromolecules on the CNPs surface [9].

In addition, there is a surface modification that aims to introduce charged or hydrophobic moieties on the CNP surface such as esterification, etherification (carboxymethylation), silylation, amidation, carbamation, sulfonation, and phosphorylation. Hence, the presence of an abundance of the −OH group on CNPs offers a unique platform for anchoring a wide spectrum of functional molecules such as aldehydes, carboxylic acids, and amines as well as macromolecule groups using these modifications [10]. Moreover, there are some surface modifications that can generate the anionic charges on the surface of the CNPs to produce anionic nanocellulose (ACNPs), such as carboxymethylation, sulfation, and phosphorylation. The anionic charge plays a crucial role and can act as a capping agent for the incorporation of the nanoparticles and also in enhancing compatibility, dispersion, and stability of the nanoparticles within the composite materials by preventing agglomeration. In that, the anionic charge from the nanocellulose will create repulsive forces that can reduce or prevent nanoparticles from clumping together, ensuring uniform dispersion in the matrix. The reported effective used method of surface modification for the ACNPs isolation is the carboxymethylation process [11].

Reaction time is a critical factor in the carboxymethylation process, as it directly influences the degree of substitution (DS) of anionic groups ($-CH_2COONa^+$) on the CNP surface. The DS represents the average number of hydroxyl groups per glucose unit of cellulose replaced by anionic groups. This study explores the use of OPEFB as a sustainable biomass source for synthesizing ACNPs by varying the carboxymethylation reaction times (30 min, 2, 4, 6, and 8 h). While significant research has focused on synthesizing anionic carboxymethyl cellulose using cellulose as the starting material, studies on synthesizing anionic nanocellulose – especially from nanocrystalline cellulose – remain limited. Moreover, the optimum reaction time for the carboxymethylation of nanocellulose has not been fully

explored. For carboxymethyl cellulose, the optimum reaction time typically ranges from 3 to 4 h, as shown in Table 1. However, it is unclear if this range applies to anionic nanocellulose synthesis, necessitating further investigation into the ideal reaction conditions. Given the nano-sized nature and high surface area of nanocellulose compared to cellulose, a shorter reaction time might be sufficient. Consequently, reaction times of 30 min and 2 h were included in this study, along with longer times (6 and 8 h), to determine the optimal reaction duration and identify when the overall properties of ACNPs begin to decline or indication of the optimization parameter for the formation of anionic charge.

Table 1: The reaction time of carboxymethyl cellulose from various types of biomass waste

Type of biomass waste	Starting materials	Reaction time (h)	Ref.
Sago waste	Cellulose	3	[12]
Banana peel	Cellulose	4	[13]
OPEFB	Cellulose	3	[14]
Agricultural wastes	Cellulose	8	[15]
OPEFB (stalk fibre)	Cellulose	3	[16]
Coconut fibre	Cellulose	1	[17]
OPEFB	Cellulose	4	[18]
OPEFB	Cellulose nanofibre	3	[19]
—	Cellulose acetate nanofibres	6	[20]

To address this gap, the present study aims to determine the optimum reaction time for synthesizing ACNPs. A range of reaction times was selected to ensure a comprehensive evaluation and to identify the most effective duration for achieving optimal ACNP synthesis. These ACNPs have potential applications across various fields, particularly when combined with different types of nanoparticles, such as bismuth ferrite for anionic dye degradation [21] or graphene to produce composite aerogel [22] or as an electrochemical working electrode [23] and as a stabilizer in nanofluids in thermal applications. Additionally, ACNPs can be combined with polymers like PVA to produce films suitable for optoelectronic applications, energy storage [24], and numerous other uses.

2 Materials

Sodium hydroxide (NaOH), sodium chlorite ($NaClO_2$, 80% w/w), and sodium chloroacetate ($ClCH_2COONa$) were supplied by Sigma Aldrich. Sulfuric acid (H_2SO_4, 95–97%) and glacial acetic acid (CH_3COOH, AR grade) were purchased

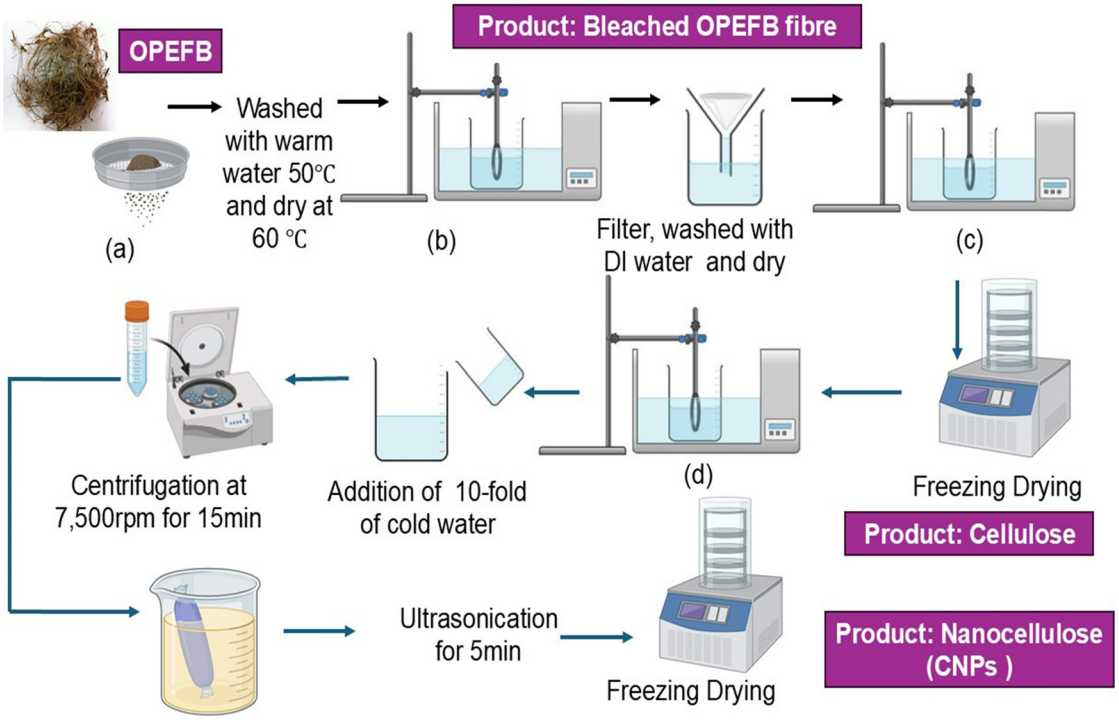

Figure 3: The three important steps in the isolation of CNPs: (a) washing and grinding of OPEFB fibre, (b) bleaching process, (c) alkaline treatment, and lastly, (d) acid hydrolysis.

from Quality Reagent Chemicals (QRec). OPEFB was taken from Oriental Rubber & Palm Oil Sdn. Bhd, Johol, Negeri Sembilan. All reagents were of analytical grade and were used without further purification. All aqueous solutions were prepared with deionized (DI) water.

3 Methodology

3.1 Nanocellulose isolation

3.1.1 Sample preparation

OPEFB was first ground using a rotor mill to fibre length around 3 mm, then sieved with 35-mesh sieves to obtain the constant fibre diameter between 2.5 and 5 mm. Then, the raw OPEFB fibres were washed with warm water (50°C) for 20 min to eliminate water-soluble impurities, as shown in Figure 3(a), and then dried in an oven at 60°C until a constant weight was attained.

3.1.2 Bleaching process

Then, the dried raw OPEFB fibre was added with 2% w/v $NaClO_2$ for the bleaching process, which was prepared by mixing equal volumes of acetate buffer (a mixture of NaOH and CH_3COOH) at pH 4, consisting of 27 g NaOH and 75 mL glacial acetic acid, diluted to 1 L with DI water as demonstrated in Figure 3(b). The bleaching process was conducted in triplicate with constant stirring for 2 h at a temperature of 80°C, utilizing an overhead stirrer at 300–400 rpm in a water bath. The treated fibre underwent a washing process with DI water until a neutral pH (6–7) was attained, and subsequently, it was dried in an oven at 60°C until a constant weight was achieved. Now, the product is referred to as bleached OPEFB fibre.

3.1.3 Alkaline treatment on bleached OPEFB fibre

After that, the bleached OPEFB fibre was treated with 4% (1.5M) NaOH solution to completely remove non-cellulosic substances (hemicellulose and lignin). This alkaline treatment was repeated three times under continuous stirring for 2 h at 80°C under constant stirring using an overhead stirrer (300–400 rpm) in a water bath, as shown in Figure 3(c). After the treatment, the resulting pulp was filtered using Whatman filter paper (pore size = 11 µm) and washed with DI water until the pulp reached pH 6–7. The retentive was collected and kept in the freezer for 24 h for freeze drying. After the freeze dry the sample is known as cellulose.

3.1.4 Acid hydrolysis on cellulose

Next, acid hydrolysis was performed using 58 wt% of H_2SO_4, with an acid-to-pulp ratio of 20 mL/g for 60 min, as illustrated in Figure 2(d). The reaction was conducted under constant stirring using an overhead stirrer (120–230 rpm) at 45°C using a water bath. Upon completion, 10 times the volume of cold water (4°C) was added to the hydrolysed mixture to stop the reaction. The mixture was then centrifuged at 7,500 rpm for 15 min to collect the sediment. The collected sediment was then dialyzed using a dialysis membrane with a molecular weight cut-off of 12,000–14,000 Da against DI water for 3–4 days until pH to 6–7. The DI water is changed every hour or daily to expedite the neutralization process. Then, the sample

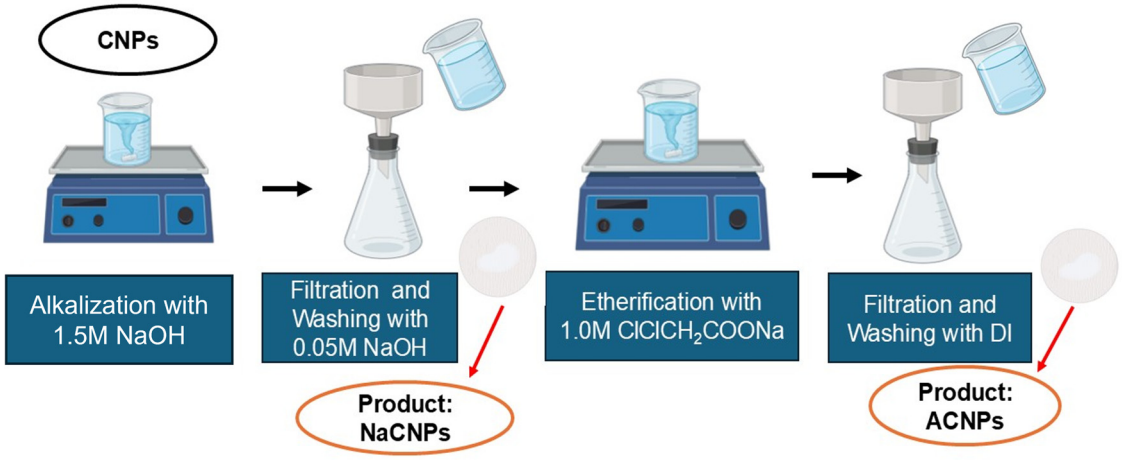

Figure 4: The steps to produce ACNPs.

was subjected to ultrasonication using a ½ in. sonication probe at 60% amplitude for 5 min in an ice bath to disperse the sample. The well-dispersed samples were frozen for 24 h before freeze-dried at −95°C for 48 h to obtain the nanocellulose, which will be denoted as CNPs.

3.2 Anionic nanocellulose isolation

The oil palm-based CNPs were first added into the 1.5 M NaOH solution and stirred constantly using the magnetic stirrer for 15 for a constant dispersion as shown in Figure 4. After 15 min, the solution was filtered using the filter paper and then washed with 0.05 M NaOH to remove the unreacted NaOH. After this process, the resultant residue will be known as sodium CNPs (NaCNPs), which will further react with 1.0 M $ClCH_2COONa$ at different reaction times starting with 30 min, then 2, 4, 6, and 8 h with constant stirring using a magnetic stirrer. Finally, the obtained anionic CNPs (ACNPs) will be washed thoroughly with DI water until pH around 6–7 and dried in air for 24 h. All this step was carried out at 25°C or room temperature.

4 Sample analysis and characterizations

Seven types of characterization were conducted to determine the optimum reaction time for the ACNPs. Structural characterization was performed using Fourier transform infrared (FTIR) (Shimadzu) and RAMAN spectroscopy (Renishaw). The chemical state and binding energy of ACNPs were analyzed by X-ray photoelectron spectroscopy (XPS) using the Axis Ultra DLD XPS (Kratos). Physical characterization included zeta potential measurement using MALVERN and particle size analysis based on transmission electron microscopy (TEM) images (ImageJ) obtained with a Zeiss Libra 120 (Germany). Finally, the crystallinity and thermal stability of the sample were evaluated using X-ray diffraction (XRD) (Bruker) and thermogravimetric analysis (TGA) analysis.

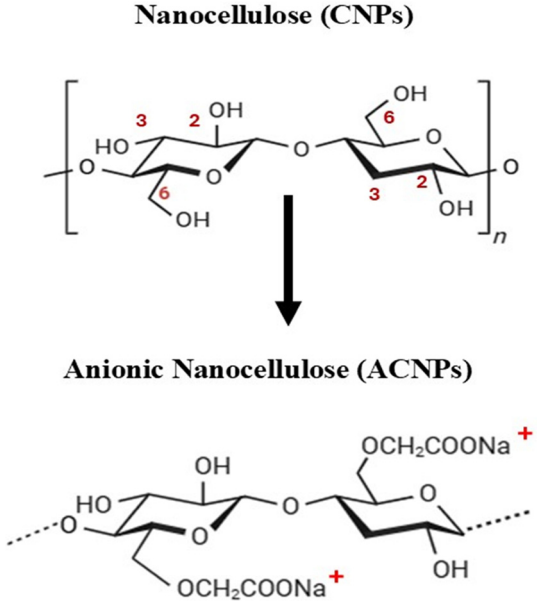

Figure 5: The synthesis of ACNPs from the CNPs *via* the carboxymethylation of the OH group.

5 Result and discussion

5.1 FTIR analysis of ACNPs

The chemical characteristics of cellulose are influenced by the sensitivity of the β-1,4-glycosidic linkages to hydrolytic attack and by the presence of three hydroxyl groups: the primary OH on C(6) and the secondary OH groups on C(2) and C(3) in the anhydroglucose units [25]. The surface modification of CNPs occurs in two phases: mercerization and carboxymethylation. During this process, some of the OH groups in the CNPs are etherified with sodium carboxymethyl groups ($-CH_2COONa$), as shown in Figure 5.

The initial stage, mercerization, serves as a swelling and impregnation phase, allowing NaOH to penetrate the cellulose matrix, forming alkaline cellulose (Na-CNPs). Na-CNPs exhibit significant reactivity with salt named sodium chloroacetate ($C_2H_2ClNaO_2$), which is then used in the subsequent carboxymethylation phase. Sodium chloroacetate is a chemical compound that contains an acetate group

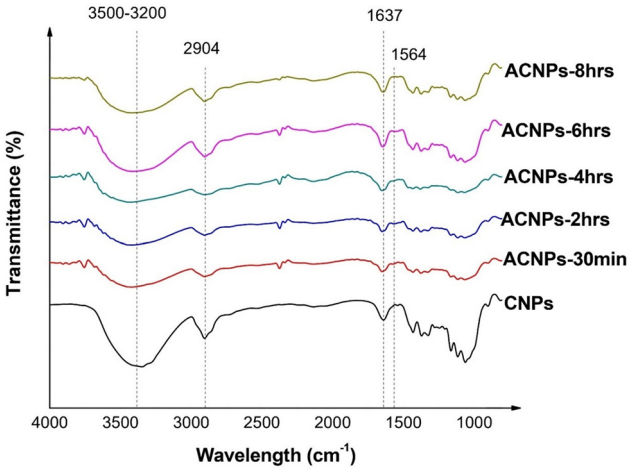

Figure 6: FTIR spectra CNPs and ACNPs at different reaction times.

(CH_2COO^-) that bonded to a chlorine atom (Cl) and the sodium ion (Na^+).

Figure 6 shows the FTIR results of the ACNPs at varying reactions. It is obvious one prominent narrow absorption peak was observed in the range of 3,348 cm^{-1}, which refers to the stretching vibration of the hydroxyl (−OH) group [26,27]. This peak refers to the intermolecular hydrogen bonding network within the CNPs chain. Another notable peak can be observed at the peak around 2,904 cm^{-1} in both CNPs and ACNPs, at all reaction times representing the stretching vibration of the C–H stretching of $-CH_2$ and $-CH_3$ groups [19]. These two peaks refer to the main polysaccharide nature, which is composed of glucose units [27]. However, −OH stretching vibration for ACNPs at different reaction times shows a wide and weak absorption band with low intensity at 3,415 cm^{-1} compared to CNPs. This is due to the low number of −OH groups in ACNPs, which can be due to the substitution of the bulky functional group ($-CH_2-COOH$) in ACNPs or the high density of the functional group [28]. In other words, the functionalization can alter the hydrogen bonding network and molecular conformation of cellulose, potentially leading to a reduction in the number of available −OH groups or changes in their accessibility. Among the functionalized samples, ACNPs-30 min, ACNPs-2 h, and ACNPs-4 h show weaker and wider band (high-intensity changes compared to CNPs (70–40%), whereas ACNPs-6 h and ACNPs-8 h (exhibit lower intensity changes compared to CNPs (55–40%). This indicates

Table 2: Comparison between the present and previous studies on the functional group that is presented according to the peak

Obtain peak (present work) cm^{-1}	Peak (wavelength) cm^{-1}	Functional group	Justification	Ref.
	1,700–1,500 cm^{-1}			
1,637, 1,564	1,640	Water absorption	The presence of the carbonyl group is confirmed	[29]
	1,585	C═O stretching		
	1,590	Asymmetric stretching vibrations of carboxylate ions ($-COO^-$)		[19]
	1,600–1,640	Carbonyl group (C═O)		[30]
	1,572	Carboxyl group (COO−) and (C–CH_2) indicating the		[20]
	1,611	presence of the sodium carboxymethyl ($-CH_2-COONa$) group		
	1,610	represents CH_2COONa		[31]
	1,606	Carbonyl group (C═O) of acetyl or carboxymethyl		[11]
	1,600 and 1,400–1,450	Carboxyl salt groups		
	1,589	Asymmetrical −COO group		[27]
	1,640	Water absorption		[17]
	1,589	Carboxylate		[18]
	1,414			
	1,565	Carboxyl group (COO−)		[32]
	1,500–1,300 cm^{-1}			
1,431, 1,379, 1,321	1,423	Symmetric stretching of the −COO group	Conforming the presence of the C–O and $-CH_2$ functional group	[27]
	1,415	Symmetric stretching vibration of carboxylate ion		[19]
	1,320	(−COO), stretching vibration of C–O		
	1,426	CH_2 scissoring and –OH bending vibration		[28]
	1,370			
	1,416	Symmetric stretching in the NaCOO group		[29]
	1,314			
	1,418	COO^- group two symmetric carboxylate stretches		[32]
	1,416			[33]
	1,324			
	1,424	$-CH_2$ bonding		[12]
	1,322	−OH plane bending		
	1,315	C–O stretch in the carboxylate functional group		[18]
	1,100–1,000 cm^{-1}			
1,064	1,061	>CH–O–CH_2 stretching, which indicates C–O–C ether linkage	Proving the presence of the ether linkage	[25]
	1,060	>CH–O–CH_2 stretching		[12]
	1,032	Ether linkages		[34]

that the OH groups in ACNPs-30 min, ACNPs-2 h, and ACNPs-4 h underwent more substantial functionalization than those in ACNPs-6 h and ACNPs-8 h. The same applies to the peak around 2,904 cm^{-1}, where ACNPs exhibit lower intensity compared to CNPs. This reduction is attributed to surface modification, which alters the number of methyl and methylene groups present on the surface of the CNPs. The replacement of some −OH groups by anionic groups or changes in the accessibility of these C–H groups leads to the observed decrease in intensity in this region. Next, the peak from 1,700 to 1,300 cm^{-1} is presented in Table 2 by comparing the peak that is present in this work with the previous study.

Next, in the range of 2,000–500 cm^{-1}, both CNPs and ACNPs exhibit similar peaks with some new peaks and changes in intensity. A sharp peak is present at 1,636 cm^{-1} in CNPs, while the ACNP spectra show peaks at 1,641–1,651 cm^{-1}, with slight intensity variations. These peaks likely correspond to the bending vibration of water molecules (H−O−H bending) [29]. Furthermore, peaks at 1,568–1,571 cm^{-1} corresponding to the asymmetric stretching vibrations of carboxylate ions ($-COO^-$) are present only in ACNPs 30 min, ACNPs-2 h, and ACNPs-4 h [19]. This observation aligns with findings from Adinugraha and Marseno [30], who noted that wavenumbers between 1,600 and 1,640 cm^{-1} represent carbonyl groups, confirming the introduction of carboxymethyl groups in CNPs during carboxymethylation. Zheng *et al.* [31] also agreed that the peak at 1,610 cm^{-1} represents CH_2COONa. Carboxyl salt groups typically appear around 1,600 cm^{-1} and between 1,400 and 1,450 cm^{-1} [11] or within the 1,500–1,700 cm^{-1} range [27]. Moreover, based on the study by Ndruru *et al.*, they point out that the peak around 1,685–1,537 cm^{-1} represents the −C═O functional group [17].

Besides that, peaks at 1,430, 1,369, 1,325 and 1,465, 1,431, 1,379, 1,321 cm^{-1} can be observed in CNP and ACNP spectra, respectively. The bending at 1,430 and 1,431 cm^{-1} for CNPs and ACNPs, respectively, represent similar functional groups, which are C–H bending vibrations in a cellulose structure. This is a common feature for cellulose and lignocellulosic materials. Furthermore, the peak at 1,379 cm^{-1} for the ACNPs corresponds to the C–H bending of CH_2 groups similar to 1,369 cm^{-1} in CNPs. Next, the peak at 1,321 cm^{-1} in ACNPs is also similar to the peak at 1,325 cm^{-1} at CNPs, which indicates the C–H bending or C–O–C stretching vibration. Those slight shifts at those peaks may be due to the effect of the anionic modification. An additional peak at ACNPs at 1,465 cm^{-1} is often associated with the CH_2 bending vibration. This additional intensity can also be influenced by the carboxylate group present. According to Suman *et al.* [28], the peak around 1,426 and 1,370 cm^{-1} in ACNPs are assigned to $-CH_2$ scissoring and –OH bending vibration, respectively. Moreover, based on the studies of Devi *et al.* [32], the band at 1,418 and 1,325 cm^{-1} is referred to COO^- group and −OH bending vibrations, respectively, whereas Zhang *et al.* [33] report that the peak around 1,416 and 1,324 cm^{-1} in the ACNPs spectrum is representing the two symmetric carboxylate stretches. Furthermore, Pushpamalar *et al.* [12] highlight that the band around 1,420 and 1,320 cm^{-1} are assigned to $-CH_2$ scissoring and −OH bending vibration, respectively.

Furthermore, peaks around 1,163, 1,114, and 1,060 and also 1,163, 1,114, and 1,064 cm^{-1} are present in the CNPs and ACNPs spectrum, respectively. Those peaks represent C–O stretching in ether. Mohamed *et al.* [19] agreed that the range group at 1,112 cm^{-1} is referring C–O–C bond stretching present along the functionalization process. Finally, the band at 1,059 cm^{-1} is due to the $>CH-O-CH_2$ stretching, which indicates C–O–C ether linkage [12,25]. This peak intensity in the ACNPs spectra is higher or stronger than at CNPs. This result was the same as discussed by Xu *et al.* [34], who synthesized the carboxymethyl cellulose nanocrystals from skimmed cotton and reported that the absorption peak of the ether band increased on functionalized CNPs. Moreover, the width of the absorption peak of ACNPs is narrower than CNPs, indicating the involvement of the hydroxyl group in the nucleophilic substitution reaction [34]. Table 2 shows the list of the peaks and corresponding functional groups.

5.1.1 Degree of substitution

From FTIR results, the calculated DS of carboxymethyl groups on the ACNPs provided insights into the optimum reaction time. The DS value represents the average number of hydroxyl groups replaced by other molecules in the polymer chain [13]. In cellulose chemistry, the reactivity of cellulose is primarily determined by its reactive groups. Specifically, the three hydroxyl groups in the anhydroglucose units of cellulose participate in substitution reactions, with the DS ranging from zero to three for each unit [35]. In the synthesis from CNPs to ACNPs, the DS refers to the number of carboxymethyl groups attached to each anhydroglucose unit [36]. Since the peak around 3,400 cm^{-1} corresponds to the −OH group, it can be compared with the C═O peak to assess the extent of carboxymethyl substitution [21]. The DS of the carboxyl group in ACNPs is determined using the following equation:

$$\mathrm{DS} = \frac{T_B - T_{1,564}}{T_B - T_{3,400}}, \tag{1}$$

where $T_{3,400}$ represents the −OH stretching, $T_{1,600}$ are related to the carboxymethyl group, and T_B is the baseline of the FTIR spectrum (100) [37]. Based on Figure 7, it is obvious that the optimum reaction time of carboxymethylation for the CNPs is 4 h due to the high DS of around 0.43, and the reaction time after the 4 h (6 and 8 h) shows low DS of around 0.26 and 0.23, respectively. This indicates that there are fewer available sites for substitution after 4 h or due to the degradation of the CNPs or the carboxymethylation agent, which can reduce the effective substitution with metal oxide.

5.2 Morphology analysis of ACNPs

Figure 8 shows the morphology of the CNPs and ACNPs at different reaction times. The morphology of the CNPs and ACNPs was similar, which is a needle-like shape as demonstrated in Figure 8(e). This indicates that the functionalization process did not affect the shape of the sample. The TEM image in Figure 8 reveals that the functionalization helps to improve the agglomeration of the CNPS, where the least agglomeration was observed in the ACNPs sample after 2 h of reaction time compared to the CNPs due to the presence of the anionic charge on the CNPs. However, after 6 h of reaction time, the ACNPs begin to agglomerate. It can be concluded that based on the TEM image, ACNPs-4 h (Figure 8(d)) and ACNPs-6 h (Figure 8(e)) show better distribution with the least agglomeration compared with ACNPs-30 min (Figure 8(b)), 2 h (Figure 8(c)), and 8 h (Figure 8(f)). This observation aligns with the findings of Li *et al.*, who synthesized cationically modified cellulose nanocrystals. They reported that surface modification of cellulose nanocrystals enhances homogeneous dispersion due to electrostatic repulsion forces, while samples with low DS tend to aggregate and form bundles [38].

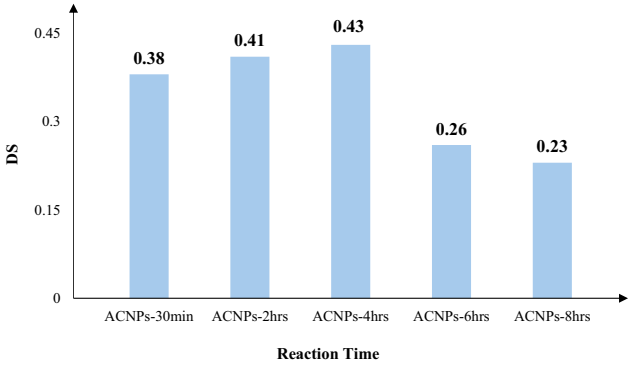

Figure 7: Degree of substitution of ACNPs at different reaction times.

Particle diameters of the ACNPs at different reaction times were measured using ImageJ (Figure 9). The diameter of the CNPs is in the range of 10–40 nm, with an average diameter of 24.46 nm. After the functionalization, the sample at reaction time 30 min and 2 h shows a similar diameter ranging from 10 to 40 nm, with average diameters of 21.95 nm and 23.81 nm, respectively. After 2 h of reaction time, the diameter of the ACNPs started to decrease with the range from 14 to 30 nm, where ACNPs-4 h, ACNPs-6 h, and ACNPs-8 h showing the average diameter of 20.90, 18.80, and 20.01 nm, respectively. This indicates that the prolonged reaction time and excessive carboxymethylation may lead to fragmentation of the CNPs, which can decrease the average diameter size of the ACNPs. Based on Figure 9, the ACNPs-4 h show the constant particle size compared to the ACNPs-6 h and ACNPs-8 h.

5.3 Zeta potential of ACNPs

The zeta potential reflects the surface charge characteristics of particles and is closely associated with the stability of the particle system. The stability of functionalized CNPs can be assessed through their zeta potential values, as shown in Table 3. A zeta potential above 30 mV is generally considered stable with minimal agglomeration. This is due to the presence of sufficient carboxylic group charges (CH_2COO^- Na^+) among ACNPs, which create repulsive forces that prevent aggregation and enhance stability. According to the zeta potential values, ACNPs-6 h exhibit the highest zeta potential at −42.8 mV, followed by ACNPs-4 h at −41.8 mV, while CNPs show the lowest value at −23.9 mV. This indicates that functionalization significantly enhances the stability of CNPs. The zeta potential findings are consistent with the TEM images, where ACNPs-4 h and ACNPs-6 h demonstrate minimal agglomeration compared to other functionalized CNPs at varying reaction times. The functionalization increases the charge density on the nanocellulose due to the introduction of carboxyl groups, resulting in a more negative zeta potential, which enhances stability by increasing repulsive forces between particles. In other words, a higher DS strengthens steric hindrance, leading to better dispersibility and stability for ACNPs [39].

5.4 TGA and DTG of ACNPs

The TGA and DTG analysis presented in Figures 10 and 11 illustrate the thermal stability and weight changes of the

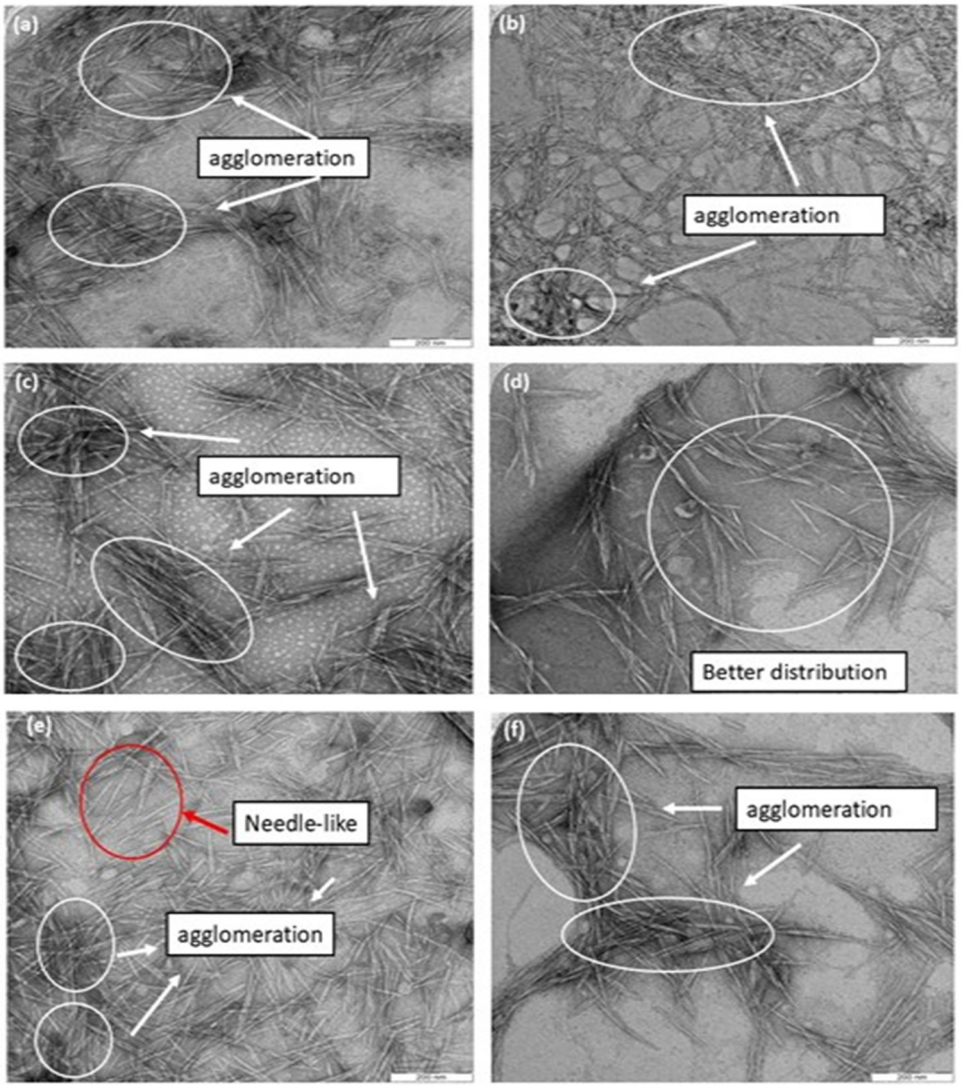

Figure 8: The TEM image at 20 KX magnification of the (a) CNPs and functionalized CNPs at different reaction times, (b) ACNPs-30 min, (c) ACNPs-2 h, (d) ACNPs-4 h, (e) ACNPs-6 h, and (f) ACNPs-8 h.

samples under inert conditions as a function of temperature. The TGA curve reveals three main stages of decomposition: the first stage occurs between 30 and 50°C, followed by the second and third stages at 250–340°C and above 400°C, respectively. Figure 11 indicates that ACNPs at different reaction times exhibit higher water/moisture content compared to CNPs. This suggests that the surface modification of CNPs increased their hydrophilicity [17]. Among the ACNPs sample, ACNPs-4 h have higher moisture content, as it has a high maximum degradation temperature (44.56°C) compared to other ACNPs.

The decomposition temperature of the CNPs started at 251.12–329.11°C, while ACNPs sample at different reaction times started decomposition at temperatures ranging from 260 to 340°C. This temperature range decomposition of ACNPs is probably owing to depolymerization, with the formation of H_2O, CO, CO_2, and CH_4 [40]. Due to the presence of COO− groups in ACNPs, decarboxylation occurs within this temperature range. This observation aligns with the findings of Mohamed *et al.* [19], who synthesized carboxymethyl cellulose nanofibres from OPEFB. They also reported that major thermal decomposition occurs above 220°C, primarily due to various degradation processes, including dehydration, decarboxylation, depolymerization, decomposition of the glycosyl units of cellulose, and the breakdown of cross-linked structures, as well as the decomposition of hydroxyl and carboxymethyl groups within the material.

In addition, the temperature at which the maximum degradation rate occurs can be used as an indicator of

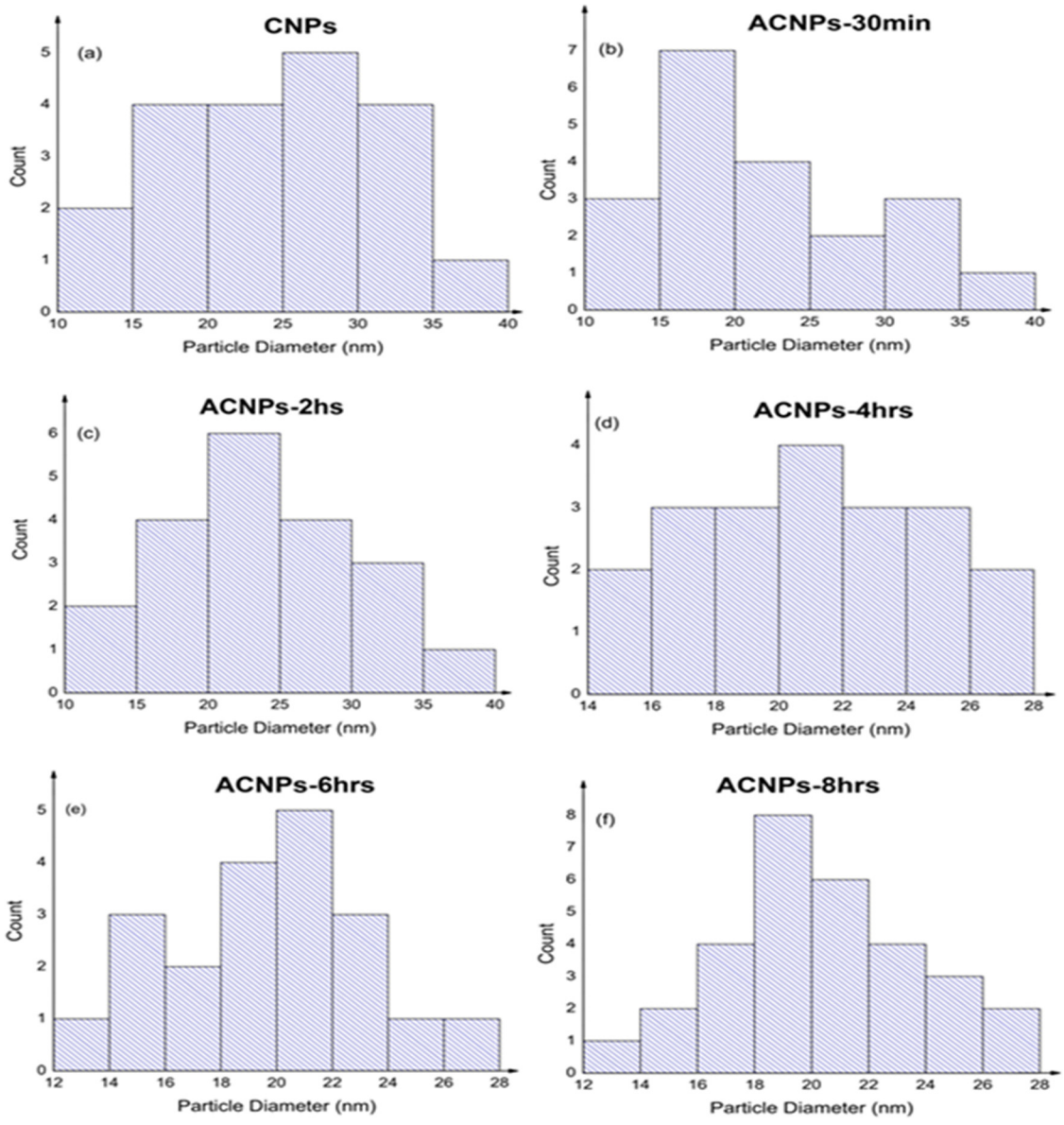

Figure 9: Particle diameter of the (a) CNPs and functionalized CNPs at different reaction times, (b) ACNPs-30 min, (c) ACNPs-2 h, (d) ACNPs-4 h, (e) ACNPs-6 h, and (f) ACNPs-8 h.

Table 3: The zeta potential value of each sample

Sample name	Zeta potential (mV)
CNPs	−23.9
ACNPs-30 min	−28.1
ACNPs-2 h	−34.4
ACNs-4 h	−41.8
ACNPs-6 h	−42.8
ACNPs-8 h	−35.2

sample's stability in comparative studies. Based on Figure 11, the maximum decomposition temperature of the ACNPs sample is higher (around 300°C) than that of CNPs (271. 54°C), indicating that the thermal stability of CNPs improves after functionalization. Besides that, relative weight (RW) refers to the weight of a sample remaining after heating to a specified temperature, expressed as a percentage of the initial weight of the sample. The information obtained from the RW in Table 4 provides insight into the thermal stability and decomposition characteristics of the materials. Higher RW% suggests better thermal stability; conversely, a lower RW% indicates a higher weight loss, suggesting more significant decomposition or degradation of the ACNPs.

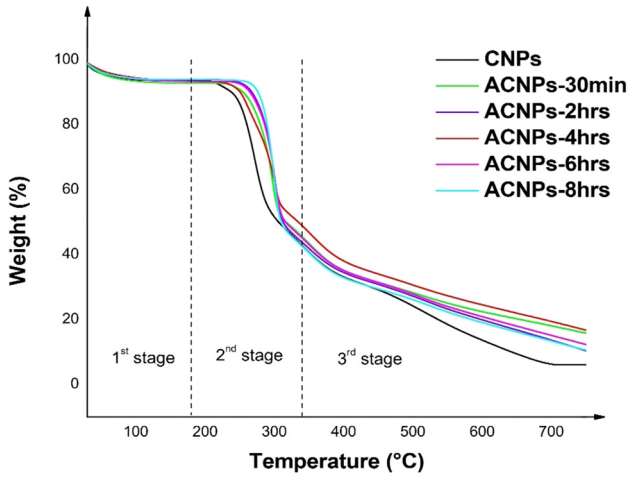

Figure 10: The TGA curve of the CNPs and the ACNPs at different reaction times.

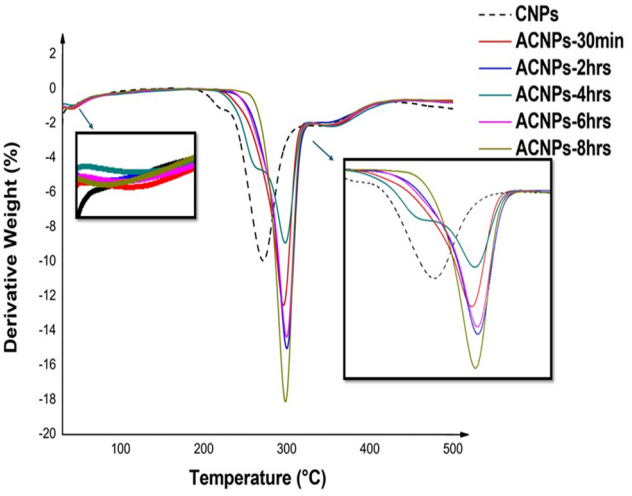

Figure 11: The DTG curve of the CNPs and the ACNPs at different reaction times.

Among the ACNPs, the highest RW%, around 13%, is owned by the ACNPs-30 min and ACNPs-4 h, and the rest ACNP shows low RW%, around 6–8%. Based on the RW result, it can be concluded that the ACNPs-30 min and the ACNPs-4 h have higher thermal stability than other ACNPs at different reaction times. However ACNPs-4hrs and ACNPs-30 showing the lowest value of T_{onset}, T_{max}, T_{end}, $T_{10\%}$, and $T_{20\%}$. This indicates that a significant portion of the materials remain after heating which is thermally stable even if the initial degradation starts at low temperature (low T_{onset}). Moreover, the lower T_{onset} and T_{end} might indicate that the materials begin to decompose at a lower temperature, but the remaining substance contributes to the high RW and is more resistant to further degradation. Another reason could be due to the DS and char. Higher DS may lead to greater distribution of the crystalline structure, potentially reducing thermal stability. This finding is in good agreement with XRD and DS data, where the ACNPs-4 h have a high DS value (around −40 mV) and also a low crystallinity index of around 77% compared to other ACNP samples. Moreover, another possibility is that the significant amount of the materials has thermally stabilized into char, indicating that some of the components including the carboxymethyl group may contribute to the formation of stable char rather than fully decomposing. This stability can be beneficial in applications where thermal resistance is desired. The reduction in the thermal stability observed could be associated with the reduction in crystallinity upon carboxymethylation [41].

5.5 Crystallinity analysis of ACNPs

The crystallinity of ACNPs from XRD is presented in Figure 12 and Table 5. According to Figure 12, the crystallinity index of the ACNPs-2 h and ACNPs-4 h is obviously lower than CNPs, from 78.22 to around 77% due to the functionalization, which broadens the cleavage of hydrogen bonds at the −OH group of cellulose and reduced the crystallinity [11]. Moreover, the main step of carboxymethylation is the formation of alkali cellulose, which can also affect the crystalline structure of cellulose. The loss of crystallinity results from the opening of the glucopyranose rings; therefore, the

Table 4: The summary of thermal stability of the CNPs and the ACNPs at different reaction times

Type of sample	T_{onset} (°C)	DTG T_{max} (°C)	T_{end} (°C)	$T_{10\%}$ (°C)	$T_{20\%}$ (°C)	RW (%) at 800°C
CNPs	251.12	271.54	329.11	238.58	260.53	6.21
ACNPs-30 min	265.86	295.97	327.36	254.95	279.87	13.51
ACNPs-2 h	277.55	300.01	338.54	267.78	287.04	6.55
ACNPs-4 h	266.66	297.97	328.70	251.04	273.96	13.86
ACNPs-6 h	275.85	299.76	339.49	265.07	286.04	8.31
ACNPs-8 h	282.63	298.35	336.89	276.59	289.70	7.65

higher the level of oxidation, the lower the degree of crystallinity [42]. Among the functionalized CNPs, the ACNPs-4 h have the lowest crystallinity intensity than other samples (Table 4). This indicates that there is high cleavage of the hydrogen bonds occurs at the −OH group, which was substituted with the carboxymethylation group into cellulose structure [43], which leads to a more amorphous structure. Moreover, the bulky carboxymethyl group on the surface of the cellulose can also reduce the ability of the cellulose chain to pack closely together.

Furthermore, high DS can further decrease crystallinity due to the increased steric hindrance, which can be absorbed in the ACNPs-4 h, indicating the optimum reaction time. Besides that, ACNPs-30 min had the high crystallinity index among the other ACNPs sample, followed by the ACNPs-6 and 8 h. This shows that, at low reaction time, the inherent structure of the cellulose, which has high and well-ordered cellulose, could be contributing to maintaining crystallinity despite the short reaction time. However, after increasing the reaction time, the crystallinity of the ACNPs started to reduce, indicating substitution of the hydroxyl group was increased and 4 h is the optimum reaction time. This is because, beyond the 4 h of reaction time of carboxymethylation, the crystallinity index of the ACNPs was almost the same as CNPs, indicating no further substitution occurred at the −OH group. The high crystallinity index of the ACNPs-6 h and ACNPs-8 h also would be the reaction for high maximum decomposition temperature.

5.6 RAMAN analysis of ACNPs

Figure 13 shows the RAMAN spectra of the CNPs and functionalized CNPs at different reaction times. The peak around 2,800–3,000 cm^{-1} represents CH stretching, and the peak around 1,430–1,480 cm^{-1} refers to vibrational modes associated with deformation or bending motions of the

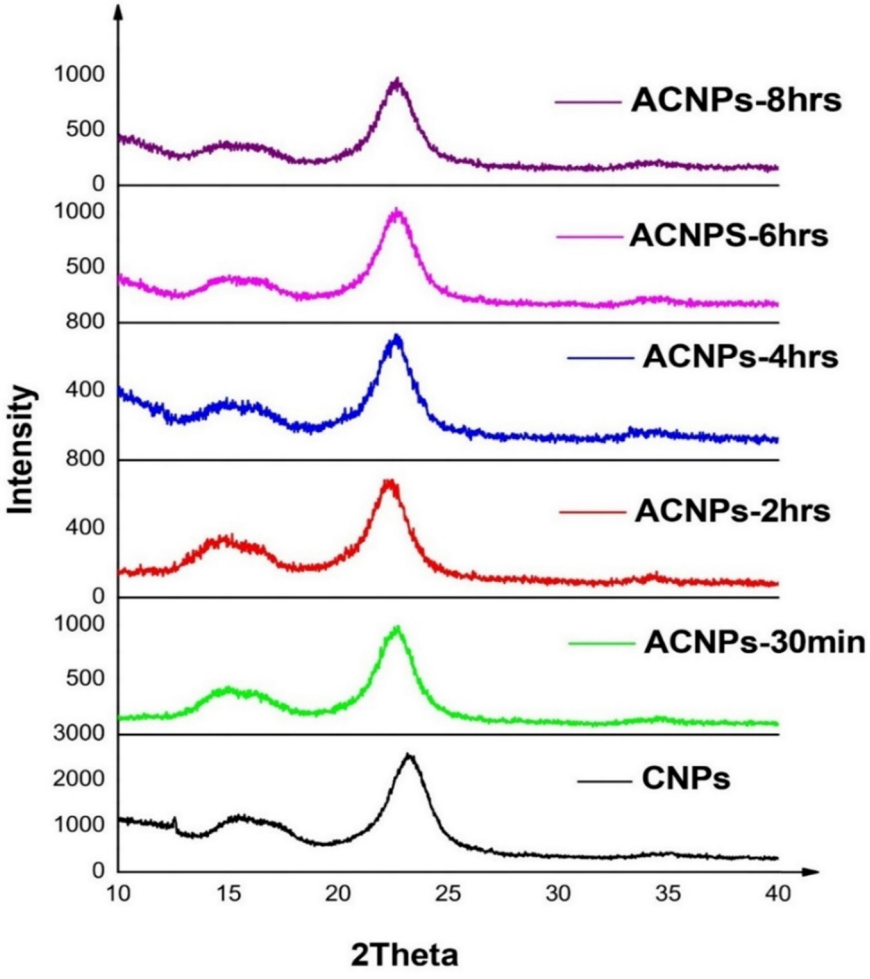

Figure 12: The XRD result of the CNPs and functionalized CNPs at different reaction times.

Table 5: The crystallinity index of CNPs and functionalized CNPs at different reaction times

Sample	Peak	Intensity of crystallinity (I_{cry})	Peak	Intensity of amorphous (I_{am})	Crystallinity index (%)
CNPs	23.15282	2,594	18.92516	565	78.22
ACNPs-30 min	22.72392	993	18.68007	182	81.67
ACNPs-2 h	22.47884	685	18.21034	151	77.96
ACNPs-4 h	22.60138	731	18.45542	168	77.01
ACNPs-6 h	22.64223	1,046	18.63923	224	78.59
ACNPs-8 h	22.7035	981	18.57796	208	78.80

molecules structure, which intensities relative to the backbone around 1,100 cm^{-1} [44]. Here, the backbone refers to the primary structure framework of the molecules, where peaks around 1,066, 1,096, 1,119, and 1,155 cm^{-1} are signals of C–O stretching or C–C bonds. The region around 1,480 cm^{-1} is assigned to the CH_2 deformation from the substitution [45], and finally peak around 2,965 cm^{-1} represents the methyl and methylene stretching.

Based on Figure 13, ACNPs-4 h is the only sample exhibiting a higher intensity than CNPs. Raman spectra display two important bands: the disorder band (D band) at approximately 1,350 cm^{-1} and the graphitic band (G band) at around 1,580 cm^{-1} [46]. The D/G ratio provides information about the DS of carboxymethyl groups on the CNPs. A high D band intensity indicates increased disorder or defects introduced into the CNPs, correlating with a higher DS of carboxymethyl groups.

In other words, the higher the D/G ratio, the greater the DS of carboxymethyl groups, and vice versa. According to Table 6, the lowest D band intensity is observed in ACNPs-8 h (3891.86), while the highest D band intensity is found in ACNPs-4 h (939,820.28). This suggests that ACNPs-4 h has the highest level of structural disorder among the ACNP samples. Furthermore, ACNPs-4 h also exhibits the highest D/G ratio, confirming that it has the highest DS of carboxymethyl groups.

5.7 XPS analysis of ACNPs

In functionalized CNPs, there are three primary elements, which are C 1s, O 1s, and Na 1s, as shown in Figure 14. The C 1s is around 284.8–286.5 eV, O 1s around 532–533 eV, and lastly, Na 1s around 1,071 eV.

From the XPS results, the type of C 1s and O 1s functional groups was plotted as shown in Figure 15(a)–(c) for the C 1s, O 1s, and Na 1s, respectively. By referring to the binding energy of the C–C/C–H assigned at 284.7 and the peak at 286.1 and 287.5 eV are attributed to C–O and C═O groups, respectively [47,48]. Next, based on O 1s spectra,

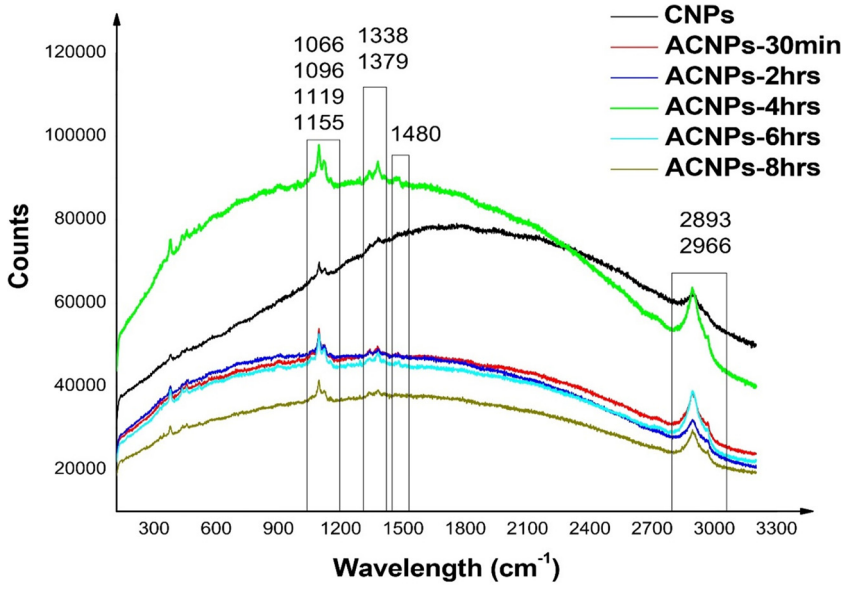

Figure 13: The RAMAN spectra of the CNPs and functionalized CNPs at different reaction times.

Table 6: The ratio of band D and band G of CNPs and ACNPs at different reaction times

Sample	Band D (1,379)	Band G (1,480)	Ratio D/G
CNPs	75801.74	76634.34	0.9891
ACNPs-30 min	49283.80	47597.38	1.0354
ACNPs-2 h	48709.27	47458.91	1.0263
ACNPs-4 h	93982.28	89481.51	1.0503
ACNPs-6 h	47987.71	46135.14	1.0402
ACNPs-8 h	38917.86	37832.53	1.0287

binding energies at 531.5 and 532.4 eV are assigned to the C–OH and C═O, respectively [20,48]. In addition, a new peak at 1070.1 eV was observed, which corresponds to the photoemission from Na^+ [28]. Based on Figure 15(c), XPS results of Na 1 s clearly confirmed the successful functionalization of CNPs, occurring in the ACNPs-4 h, ACNPs-6 h, and ACNPs-8 h, due to the presence of the peak. However,

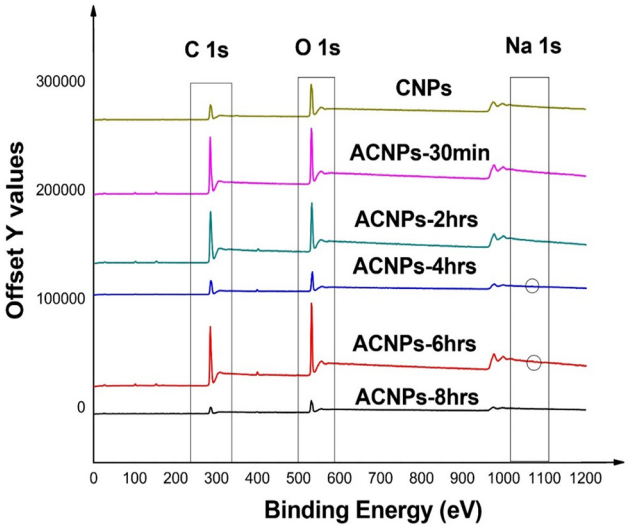

Figure 14: The three important key elements in the functionalized CNPs.

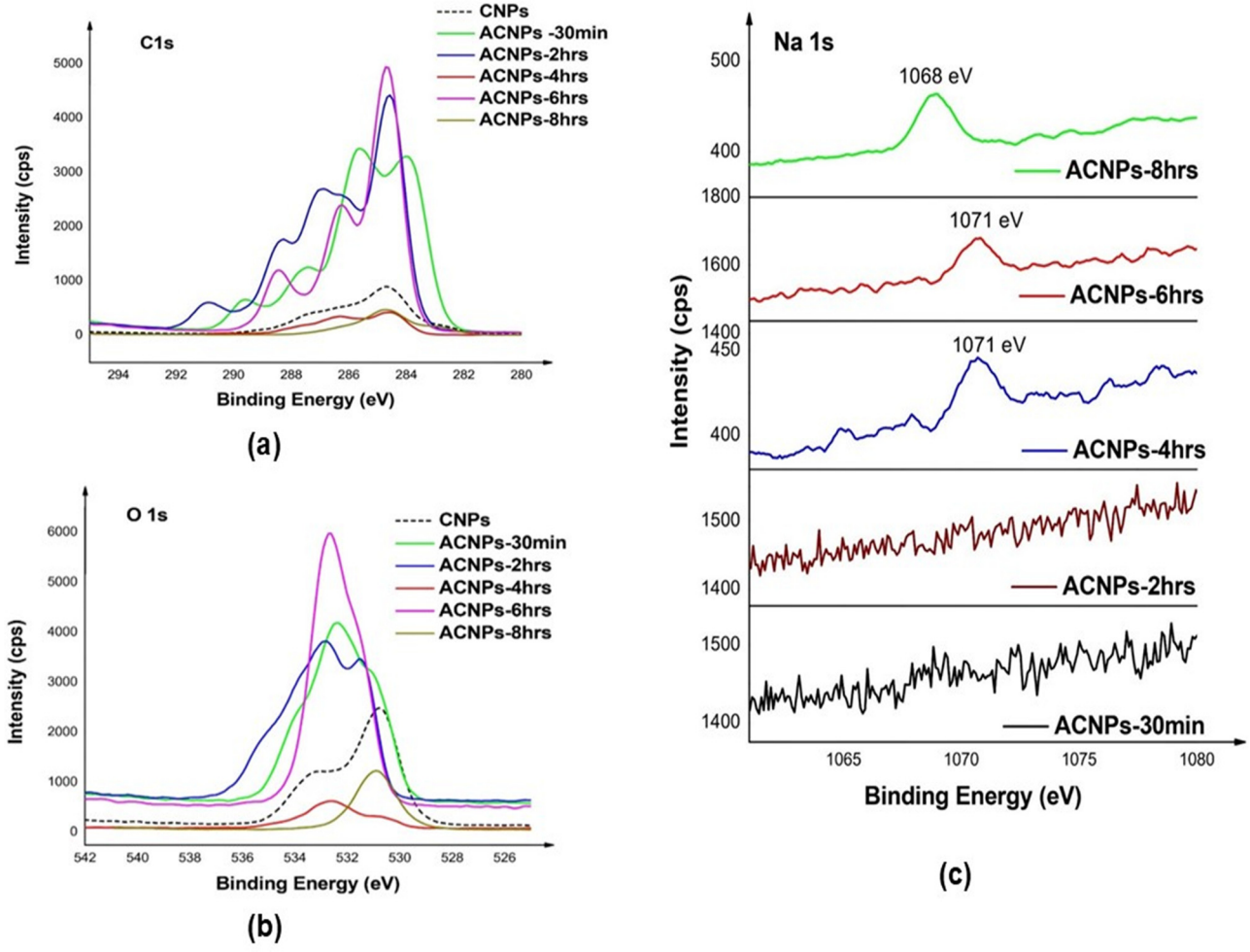

Figure 15: The (a) C 1s, (b) O 1s, and (c) Na 1s binding energy *versus* intensity spectra of CNP and ACNPs at different reaction times.

Table 7: The binding energy and the atomic mass concentration of C 1s, O 1s, and Na 1s

Type of sample	C 1s Atomic concentration (%)	O 1s Atomic concentration (%)	Na 1s Atomic concentration (%)
CNPs	49.98	49.17	—
ACNPs-30 min	67.27	30.73	—
ACNPs-2 h	72.13	25.43	—
ACNPs-4 h	78.07	17.80	0.50
ACNPs-6 h	65.29	30.82	0.16
ACNPs-8 h	48.87	48.68	0.21

ACNPs-4 h and ACNPs 6 h had the peak at 1,071 eV, but ACNPs-8 h had Na 1s peak at 1,068 eV. The shift in Na 1s binding energy from 1,071 eV in ACNPs-4 h and ACNPs-6 h to 1,068 eV in ACNPs-8 h suggests that the sodium ions (Na^+) in ACNPs experience a change in their chemical environment with increasing reaction time. At 4 and 6 h, the sodium ions may be more strongly coordinated or bound to the CNPs backbone, resulting in higher binding energy, as more energy is required to remove an electron from a tightly bound ion. In contrast, at ACNPs-8 h, where the ions are less tightly bound, it becomes easier to remove an electron, resulting in a lower binding energy. Furthermore, the 0% atomic mass of Na 1s, as shown in Table 7, indicates the absence of Na^+ in ACNPs-30 min and ACNPs-2 h. Among ACNPs-4 h, ACNPs-6 h, and ACNPs-8 h, ACNPs-4 h has the highest Na atomic concentration, suggesting that 4 h may be the optimal reaction time for carboxymethylation, as supported by the Raman and DS results.

According to Table 6, the atomic concentration of O 1 s in CNPs is 49.17%. After carboxymethylation, however, the atomic concentration of O 1s decreases. Among the samples, ACNPs-4 h has the lowest O 1s concentration (17.80%), while ACNPs-8 h remains nearly unchanged at 48.68%. Because in ACNPs, the $-CH_2COONa$ group attaches to the cellulose backbone by replacing the OH groups. When the DS of $-CH_2COONa$ groups in CNPs is high, there are more −COONa groups and fewer OH groups, leading to reduced oxygen intensity. This results in a lower O 1s signal, as fewer hydroxyl groups are available to contribute to the oxygen peak. Additionally, the low O 1s concentration may be due to the substitution of cellulose's −OH groups with ether linkages in ACNPs, decreasing the number of oxygen atoms directly associated with the cellulose structure. These changes confirm the successful functionalization of the CNPs. This result aligns with FTIR findings, where the −OH peak shows weaker intensity in ACNPs compared to CNPs, indicating a reduced number of OH groups.

The atomic concentration of C 1s in ACNPs was higher than in CNPs. However, at ACNPs-8 h, the atomic concentration was similar to that in CNPs, with ACNPs-4 h showing the highest concentration (78.01%). This increase is likely due to the substitution of −OH groups with ether linkages, which contributes additional carbon atoms to the structure. Additionally, based on Na 1s data, it is evident that carboxymethylation begins after 2 h of reaction time. Consequently, ACNPs-4 h, ACNPs-6 h, and ACNPs-8 h show varying Na atomic concentrations, with ACNPs-4 h having the highest concentration (0.50%), followed by ACNPs-8 h (0.21%) and ACNPs-6 h (0.16%). While extended reaction time can optimize certain transformations, it may also reduce Na 1s atomic concentration due to possible decomposition or side reactions. Longer reaction times might promote unwanted reactions or decomposition, altering the sample's composition and ultimately decreasing sodium concentration.

6 Conclusion

In conclusion, FTIR characterization reveals a decrease in the intensity of the −OH and C–H peaks in the ACNP samples compared to CNPs, indicating successful surface modification. This reduction is attributed to the extended carboxymethylation time, enhancing the interaction between chloroacetic acid and cellulose hydroxyl groups. Additional peaks around 1,600 and 1,400–1,450 cm^{-1} in the FTIR spectra confirm the carboxymethylation of CNPs, corresponding to the carboxylate group (COO^-) and the stretching and deformation vibrations of methyl ($-CH_3$) groups. Among the samples, ACNPs-4 h exhibits the highest DS at 0.43, indicating the most significant substitution of −OH groups with anionic groups during the 4-h reaction time. TEM analysis shows that the needle-like shape of CNPs is retained after functionalization, demonstrating that surface modification does not alter the morphology of the particles. While surface modification improves particle distribution for up to 2 h, ACNPs begin to agglomerate beyond 4 h. ACNPs-4 h demonstrates the best particle distribution and uniform particle diameter, confirming it as the optimum reaction time. Thermal stability analysis

using TGA and DTG shows improved stability in ACNPs after functionalization. XRD analysis reveals a lower crystallinity index for ACNPs compared to CNPs due to structural modifications, with ACNPs-4 h exhibiting the lowest crystallinity index among all samples. Raman spectroscopy further supports these findings, with ACNPs-4 h displaying the highest D/G band ratio (1.0503), reflecting greater substitution of carboxymethyl groups. This aligns with zeta potential measurements, where ACNPs-4 h achieves a value of −41.8 mV, indicating excellent dispersion and uniform particle size. Finally, XPS analysis confirms ACNPs-4 h as the optimum reaction time, evidenced by the highest concentration of sodium ions (Na^+) in the Na 1s spectra (0.50%), compared to ACNPs-6 h (0.16%) and ACNPs-8 h (0.21%). Based on these results, ACNPs-4 h is identified as the optimal sample that offers superior substitution, distribution, thermal stability, and structural properties for further hybridization with metal oxide that has cationic characteristics.

Acknowledgments: Special thanks to the Ministry of Higher Education (MOHE) for funding under the Fundamental Research Grant Scheme (FRGS) (FRGS/1/2023/STG05/USM/02/3). The authors would like to express gratitude for the financial support received from the Universiti Pertahanan Nasional Malaysia.

Funding information: Fundamental Research Grant Scheme (FRGS) (FRGS/1/2023/STG05/USM/02/3).

Author contributions: Conceptualization, writing-original draft preparation, review, and editing: Mageswari Manimaran, Mohd Nurazzi Norizan, Mohd Nor Faiz Norrrahim; conceptualization: Mohamad Haafiz Mohamad Kassim, Mohd Ridhwan Adam, Norli Abdullah. All authors have accepted responsibility for the entire content of this manuscript and approved its submission.

Conflict of interest: The authors state no conflict of interest.

Data availability statement: All data generated or analyzed during this study are included in this published article.

References

[1] Parveez Ghulam Kadir A. Overview of the malaysian oil palm industry in 2023. Malaysia: Malaysian Palm Oil Board (MPOB); 2023. p. 2022–4.

[2] Su G, Wahidah N, Zulkifli M, Chyuan H, Ibrahim S. Pyrolysis of oil palm wastes for bioenergy in Malaysia: A review. Renew Sustain Energy Rev. 2022;164:112554. doi: 10.1016/j.rser.2022.112554.

[3] Lim HJ, Cheng WK, Tan KW, Yu LJ. Oil palm-based nanocellulose for a sustainable future: Where are we now? J Env Chem Eng. 2022;10(2):107271. doi: 10.1016/j.jece.2022.107271.

[4] Aigaje E, Riofrio A. Processing, properties, modifications, and environmental impact of nanocellulose/biopolymer composites: a review. Polymers. 2023;15:1–36.

[5] Lamaming J, Hashim R, Leh CP, Sulaiman O, Lamaming SZ. Bionanocomposite Films reinforced with various types of cellulose nanocrystals isolated from oil palm biomass waste. Waste Biomass Valoriz. 2020;11(12):7017–27. doi: 10.1007/s12649-019-00892-7.

[6] Yang X, Biswas SK, Han J, Tanpichai S, Li MC, Chen C, et al. Surface and interface engineering for nanocellulosic advanced materials. Adv Mater. 2021;33(28):1–30.

[7] Oprea M, Mihaela Panaitescu D. Nanocellulose hybrids with metal oxides nanoparticles for biomedical applications. Molecules. 2020;25(18):4–6.

[8] Oun AA, Shankar S, Rhim JW. Multifunctional nanocellulose/metal and metal oxide nanoparticle hybrid nanomaterials. Crit Rev Food Sci Nutr. 2020;60(3):435–60.

[9] Peng S, Luo Q, Zhou G, Xu X. Recent advances on cellulose nanocrystals and their derivatives. Polymers. 2021;13(19):1–34.

[10] Ghasemlou M, Daver F, Ivanova EP, Habibi Y, Adhikari B. Surface modifications of nanocellulose: From synthesis to high-performance nanocomposites. Prog Polym Sci. 2021;119:101418. doi: 10.1016/j.progpolymsci.2021.101418.

[11] Rasid NSA, Zainol MM, Amin NAS. Synthesis and characterization of carboxymethyl cellulose derived from empty fruit bunch. Sains Malaysiana. 2021;50(9):2523–35.

[12] Pushpamalar V, Langford SJ, Ahmad M, Lim YY. Optimization of reaction conditions for preparing carboxymethyl cellulose from sago waste. Carbohydr Polym. 2006;64(2):312–8, https://www.sciencedirect.com/science/article/pii/S0144861705006041.

[13] Flour W, Cui Z, Gao X, He X, Xiang X, Melts TC, et al. Effects of reaction time on degree of substitution, yield and morphology of carboxymethyl cellulose from banana peel. IOP Publishing, 21st International Union of Materials Research Societies International Conference in Asia, 23–26 February 2021, Chiang Mai, Thailand; 2022.

[14] Tuan Mohamood NFA-Z, Abdul Halim AH, Zainuddin N. Carboxymethyl cellulose hydrogel from biomass waste of oil palm empty fruit bunch using calcium chloride as crosslinking agent. Polymers. 2021;13(23):1–16.

[15] Moussa I, Khiari R, Moussa A, Belgacem MN. Preparation and characterization of carboxymethyl cellulose with a high degree of substitution from agricultural wastes. 2019;20:933–43.

[16] Parid DM, Aliaa N, Rahman A, Baharuddin AS, Mohammed MAP. Synthesis and characterization of carboxymethyl cellulose from oil palm empty fruit bunch stalk fibres. BioResources. 2018;13(1):535–54.

[17] Ndruru ST, Amri N, Kusuma SB, Prasetyo R, Hayati AT, Mawarni RS, et al. Facile synthesis of carboxymethyl cellulose from Indonesia's coconut fiber cellulose for bioplastics applications. Polym Eng Sci. 2024;64(9):4144–60.

[18] Yimlamai B, Choorit W. Cellulose from oil palm empty fruit bunch fi ber and its conversion to carboxymethylcellulose. J Chem Technol Biotechnol. 2021;96:1656–66.

[19] Mohamed AH, Yahaya N, Mohamad S, Kamaruzaman S, Osman H, Nishiyama N, et al. Synthesis of oil palm empty fruit bunch-based magnetic-carboxymethyl cellulose nanofiber composite for magnetic solid-phase extraction of organophosphorus pesticides in environmental water samples. Microchem J. 2022;183:108045. doi: 10.1016/j.microc.2022.108045.

[20] Gopiraman M, Bang H, Yuan G, Yin C, Song K-H, Lee JS, et al. Noble metal/functionalized cellulose nanofiber composites for catalytic applications. Carbohydr Polym. 2015;132:554–64, https://www.sciencedirect.com/science/article/pii/S0144861715005603.
[21] Md Azman SAH, Sagadevan S, Ahmad I, Kassim MHM, Imam SS, Nguyen KD, et al. Integration of carboxymethyl cellulose isolated from oil palm empty fruit bunch waste into bismuth ferrite as photocatalyst for effective anionic dyes degradation. Catalysts. 2022;12(10):1–17.
[22] Xu W, Chen S, Zhu Y, Xiang X, Bo Y, Lin Z, et al. Preparation of hyperelastic graphene/carboxymethyl cellulose composite aerogels by ambient pressure drying and its adsorption applications. J Mater Sci. 2020;55(24):10543–57. doi: 10.1007/s10853-020-04720-5.
[23] Nanoparticles CA. Carboxymethyl-cellulose-containing Ag nanoparticles as an electrochemical working electrode for fast hydroxymethyl-furfural sensing in date molasses. Polymers. 2022;15(1):79.
[24] Abouhaswa AS, Turky GM, Soliman TS. Structural, optical, and dielectric properties of PVA-CMC/Ni0.65Cu0.35Fe2O4 films for optoelectronic applications and energy storage applications. J Inorg Organomet Polym Mater. 2024;34(4):1699–711. doi: 10.1007/s10904-023-02911-6.
[25] Eliza MY, Shahruddin M, Noormaziah J, Rosli WDW. Carboxymethyl Cellulose (CMC) from oil palm empty fruit bunch (OPEFB) in the new solvent dimethyl sulfoxide (DMSO)/tetrabutylammonium fluoride (TBAF). J Phys Conf Ser. 2015;622(1):1–10.
[26] Kaewprachu P, Jaisan C, Rawdkuen S, Tongdeesoontorn W, Klunklin W. Carboxymethyl cellulose from Young Palmyra palm fruit husk: Synthesis, characterization, and film properties. Food Hydrocoll. 2022;124:107277. https://www.sciencedirect.com/science/article/pii/S0268005X21006937.
[27] Tuan Mohamood NFAZ, Abdul Halim AH, Zainuddin N. Carboxymethyl cellulose hydrogel from biomass waste of oil palm empty fruit bunch using calcium chloride as crosslinking agent. Polym (Basel). 2021;13(23):1–16.
[28] Suman, Awasthi D, Bajaj B. Influence of rice straw based nanocellulose loading in sodium carboxymethyl cellulose. Mater Today Proc. 2024. doi: 10.1016/j.matpr.2024.05.084.
[29] Fernández-Santos J, Valls C, Cusola O, Roncero MB. Composites of cellulose nanocrystals in combination with either cellulose nanofibril or carboxymethylcellulose as functional packaging films. Int J Biol Macromol. 2022;211:218–9.
[30] Adinugraha MP, Marseno DW. Synthesis and characterization of sodium carboxymethylcellulose from cavendish banana pseudo stem (Musa cavendishii LAMBERT). Carbohydr Polym. 2005;62(2):164–9, https://www.sciencedirect.com/science/article/pii/S0144861705003176.
[31] Zheng M, Su H, Xiao R, Chen J, Chen H, Tan KB, et al. Effects of Polygonatum cyrtonema extracts on the antioxidant ability, physical and structure properties of carboxymethyl cellulose-xanthan gum-flaxseed gum active packaging films. Food Chem. 2023;403:134320, https://www.sciencedirect.com/science/article/pii/S0308814622022828.
[32] Devi BL, Rao KM, Ramananda D. Spectroscopic investigation of green synthesized ZnS nanoparticles encapsulated by sodium carboxy methyl cellulose. Appl Phys A Mater Sci Process. 2020;126(12):1–11. doi: 10.1007/s00339-020-04107-y.
[33] Zhang F, Dou J, Zhang H. Mixed membranes comprising carboxymethyl cellulose (as capping agent and gas barrier matrix) and nanoporous ZIF-L nanosheets for gas separation applications. Polymers (Basel). 2018;10(12):1–15.
[34] Xu T, Li A, Zheng X, Ji B, Mei J, Zhou M, et al. Porous carboxymethyl cellulose nanocrystalline imprinted composite aerogels for selective adsorption of gadolinium. Chemosphere. 2024;349:140931. doi: 10.1016/j.chemosphere.2023.140931.
[35] Rahman MS, Hasan MS, Nitai AS, Nam S, Karmakar AK, Ahsan MS, et al. Recent developments of carboxymethyl cellulose. Polym (Basel). 2021;13(8):1–48.
[36] Gargey IA, Indira D, Jayabalan R, Balasubramanian P. Optimization of etherification reactions for recycling of tea fungal biomass waste into carboxymethylcellulose. Singapore: Springer; 2019. p. 337–46. doi: 10.1007/978-981-13-1202-1_29.
[37] Adolph R. Thermal degradation of poly(vinyl chloride): Effect of nanoclay and low density polyethylene content. Iran Polym J. 2016;20:1–23.
[38] Li M, Mei C, Xu X, Lee S, Wu Q. Cationic surface modi fi cation of cellulose nanocrystals: Toward tailoring dispersion and interface in carboxymethyl cellulose films. Polym (Guildf). 2016;107:200–10. doi: 10.1016/j.polymer.2016.11.022.
[39] Zhang X, Xi C, Guo S, Yan M, Lu Y, Sun Z, et al. Electron beam pre-irradiation enhances substitution degree, and physicochemical and functional properties of carboxymethyl peanut shell nanocellulose. Ind Crop Prod. 2024;209:118035. doi: 10.1016/j.indcrop.2024.118035.
[40] Yeasmin S. Synthesis of carboxymethyl cellulose from corn leaves based on particle size - a new aspect. New York, NY, USA: Nova Science; Vol. 2092, 2008. p. 92113–13.
[41] Casaburi A, Montoya Rojo Ú, Cerrutti P, Vázquez A, Foresti ML. Carboxymethyl cellulose with tailored degree of substitution obtained from bacterial cellulose. Food Hydrocoll. 2018;75:147–56.
[42] Tavares KM, Campos A, de, Luchesi BR, Resende AA, Oliveira JE, de, Marconcini JM. Effect of carboxymethyl cellulose concentration on mechanical and water vapor barrier properties of corn starch films. Carbohydr Polym. 2020;246:116521. doi: 10.1016/j.carbpol.2020.116521.
[43] Kaczmarska K, Grabowska B, Spychaj T, Zdanowicz M, Sitarz M, Bobrowski A, et al. Effect of microwave treatment on structure of binders based on sodium carboxymethyl starch: FT-IR, FT-Raman and XRD investigations. Spectrochim Acta - Part A Mol Biomol Spectrosc. 2018;199:387–93. doi: 10.1016/j.saa.2018.03.047.
[44] Moura HOMA, de Souza EC, Brendo R, Pereira ES, Bicudo TDC, Rodríguez-castell E. Industrial crops & products optimization of synthesis method for carboxymethylcellulose (CMC) from agro-food wastes by response surface methodology (RSM) using D-optimal algorithm. Industrial Crops and Products. 2024;220:119413.
[45] Adar F. Characterizing modified celluloses using raman spectroscopy. Spectrosc (St Monica). 2016;31(11):22–7.
[46] Sufi S, Chaudhary K, Haider Z. Effect of magnetic field on carbon nanotubes and graphene structure synthesized at low pressure via arc discharge process. AIP Publishing, International Conference on Plasma Science and Applications (ICPSA 2016), 28–30 November 2016, Langkawi – Malaysia; 2017.
[47] Zhao M, Zhang S, Fang G, Huang C, Wu T. Directionally-grown carboxymethyl cellulose/reduced graphene oxide aerogel with excellent structure stability and adsorption capacity. Polymers (Basel). 2020;12(10):1–15.
[48] Zhang F, Dou J, Zhang H. Mixed membranes comprising carboxymethyl cellulose (as capping agent and gas barrier matrix) and nanoporous Z-L nanosheets for gas separation applications, Zhang H. Mixed membranes comprising carboxymethyl cellulose (as capping agent and gas barrier matrix) and nanoporous ZIF-L nanosheets for gas separation applications. Polymers (Basel). 2018;10(12):1–15.